

# THE EFFECT OF SUPERPARAMETERIZATION ON AEROSOL TRANSPORT

W. C. Hsieh, D. Rosa and W. D. Collins  
University of California, Berkeley, California

## 1. INTRODUCTION

Understanding earth system and interactions among its internal components is essential to predict climate change. Within the framework of general circulation models (GCMs), sub-grid scale processes are known to be among the most important and uncertain components for correct climate predictions. Aerosols represent one of the most uncertain agents altering the Earth's energy budget and are strongly affected by sub-grid processes in GCMs. The climate community recognizes that modeling sub-grid processes and ways how they interact with large-scale circulations is important for a more realistic climate prediction, but until recently it has lacked a framework for quantitatively exploring these issues [5]. In the last few years, a new multiscale modeling framework (MMF) has developed to simulate explicitly the cloud-scale processes inside each column of a GCM [4]. For each grid cell, the physics, thermodynamics and small-scale dynamics are explicitly simulated by a cloud-resolving model (CRM), which replaces the traditional conventional cloud parameterizations. This MMF method is also called as a superparameterization (SP) for clouds and such framework has been integrated into the NCAR Community Atmosphere Model (CAM) to study interannual and subseasonal variability of climate [2].

The CRM generates clouds and their effects on the environment, including the mixing and advection of chemical species, without employing the highly empirical and conventional cloud parameterizations used in traditional GCMs. In this study, we would use this superparameterization CAM (SPCAM) to investigate the effects of SPCAM framework on aerosol transport where mineral dust is studied first. Modeling transports of chemical constituents are determined by several factors, such as numerical schemes for dynamical processes, patterns of simulated wind and mass fields, and subgrid scale parameterizations [6]. This paper focuses on the last component, namely, the representation of subgrid scale processes in transport problems in GCMs. Following the physical processes of water vapor modeled in the SP framework used in this study, we implemented four dust bins from CAM in SPCAM. More details of dust implementation is discussed in

the Section 3. There is much room for improvement of dust implementation in SPCAM, and the analysis here should be considered as a first estimate.

## 2. GENERAL MODEL DESCRIPTION

The SPCAM used in this study was developed by [4] and the version of SPCAM we used is based on CAM 3.5.11 which was used as a host GCM. The general formula and simulation results of CAM version 3 were documented in [1]. The CAM was configured to run at  $1.9^\circ \times 2.5^\circ$  horizontal resolution with a total of 28 vertical layers. The time step of CAM is 900 s and the finite volume dynamical core was used for all simulations. The SP component of SPCAM is a 2D CRM, which was arranged in the east-west orientation with 26 levels collocated with the GCM vertical layers. There are 32 columns for the CRM domain in each grid cell of GCM, with 4 km horizontal grid size. The time step of CRM is 20 s. The CRM solved the nonhydrostatic dynamical equations with anelastic approximation and used a finite-difference method to represent prognostic equations in flux forms. The model applied the second-order central-difference to compute advection of momentum with kinetic energy conservation. The model employed the positively defined monotone algorithms for advection of all prognostic scalars, which include the liquid water/ice moist static energy, total nonprecipitating water (vapor + cloud water + cloud ice), and total precipitating water (rain + snow + graupel). More details of the CRM were described in [3].

## 3. COUPLING BETWEEN SP AND CAM FOR DUST

The implementation of dust in SPCAM follows the SPCAM model developed by [4], and sub-grid scale transport of dust in CRM model is based on treatment of water vapor transport by SPCAM. The details of SPCAM is described by [4], here we only mention some changes made to coupling between SP and CAM for the implemented dust component. In the original SPCAM, the tendency of large scale forcing exerted in small scale CRM is

calculated as [4]:

$$\left[ \frac{\partial \Psi}{\partial t} \right]_{LS} = \frac{\Psi_{CAM} - \bar{\Psi}^n}{\Delta t_{CAM}} \quad (1)$$

where  $\Psi$  is the SP prognostic variable, which can be water vapor, cloud condensate and dust, the focus of this study.  $\Psi_{CAM}$  is the corresponding CAM variable,  $\bar{\Psi}^n$  is the horizontal mean SP variable at the previous CAM time step  $\Delta t_{CAM}$ . This term is computed at the beginning of the CRM call and is fixed though the whole integration by CRM within CAM time step. However, in this study, the tendency of large scale forcing for dust is calculated in each time step of CRM such that the updated  $\bar{\Psi}^n$  in CRM is used to compute Equation (1). This implementation still remains the property that SP mean fields follow the corresponding CAM fields but is more reliable in numerical realizations for dust simulations. The feedback of small scale processes to the large scale CAM variables is computed at the end of CRM call and is the same formula provided in[4]:

$$\left[ \frac{\partial \Psi}{\partial t} \right]_{SS} = \frac{\bar{\Psi}^{n+1} - \Psi_{CAM}}{\Delta t_{CAM}} \quad (2)$$

where  $\bar{\Psi}^{n+1}$  is the last step of horizontally averaged SP fields at the end of CRM call.

#### 4. EXPERIMENT SETUP

For the setup of the current experiments, both CAM and SPCAM were configured in the chemical transport mode such that the inputs of meteorology are identical in both simulations. This can avoid the uncertainty from difference in online meteorology thus the differences of dust fields between CAM and SPCAM are attributed to the difference in the treatment of sub-grid scale processes. All simulations started at Feb, 2, 2000 and were run for one month with hourly outputs of the specified variables. Both models were setup in NCAR bluefire supercomputer which is an IBM clustered Symmetric MultiProcessing (SMP) system based on the Power6 chip. In current version of CAM, four dust bins are computed, including DST01, DST02, DST03, and DST04 with the corresponding diameter range are 0.1 - 1.0  $\mu\text{m}$ , 1.0 - 2.5  $\mu\text{m}$ , 2.5 - 5.0  $\mu\text{m}$  and 5.0 - 10.0  $\mu\text{m}$ , respectively. In the CAM used in this study, modeling dust distributions is based on the Mineral Dust Entrainment and Deposition (DEAD) model, developed by Zender et al. (2003) [7]. In this study, only molecular-scale

diffusion and small-scale advection of dust are included in SPCAM. The removal of dust such as dry/wet deposition is still calculated in CAM which also computes large-scale transport.

#### 5. RESULTS AND DISCUSSIONS

Figure 1 shows the comparison of DST01 dust mixing ratio in the lowest layer between SPCAM (top) and CAM (bottom); the output hourly data are first averaged to the averaged daily data which are further averaged for February, 2000. In general, the spatial distributions of DST01 are similar for these two simulations, but dust concentrations in SPCAM are slightly higher in areas near the source regions and the transported dust reaches to a longer distance than CAM. For example, the dust plume originates in west Africa (0 - 17  $^{\circ}\text{W}$ , 10  $^{\circ}\text{N}$ -35  $^{\circ}\text{N}$ ) is transported southwestly; the contour plume of concentration  $>1\text{e}^{-8}$  kg/kg reaches 30  $^{\circ}\text{W}$  in SPCAM but 15  $^{\circ}\text{W}$  in CAM.

Figure 2 shows the zonal averaged mixing ratio of DST01 versus vertical height for SPCAM and CAM; data was averaged for the month of February, 2000. The overall patterns are similar between two simulations, the largest dust plume is seen in the low layers between 7  $^{\circ}\text{N}$  - 25  $^{\circ}\text{N}$  and dust concentrations are higher in the North Hemisphere, which are consistent with the global geographical dust distributions shown in Figure 1. In the region around -5  $^{\circ}\text{S}$  - 60  $^{\circ}\text{N}$ , DST01 predicted by SPCAM is transported to a higher level (300 mb in SPCAM versus 500 mb in CAM for dust mixing ratio between  $1\text{e}^{-10}$  -  $5\text{e}^{-10}$ ). There is another local high DST01 concentration around 40  $^{\circ}\text{N}$  in the lower level for SPCAM which is not significant in CAM. The corresponding meridional averaged mixing ratio of DST01 versus vertical height is shown in Figure 3. The difference between SPCAM and CAM is recognizable, for example, there is a high contour dust formed around 0 - 30  $^{\circ}\text{W}$  near surface in SPCAM and this is due to the dust originated from west Africa which is transported further west. Another noticeable difference is the region between 60  $^{\circ}\text{E}$  - 180 from level 300 - 400 mb, the DST01 simulated in SPCAM is higher than CAM from about a factor of 5 to one order of magnitude. The meridional mean plots reveal the dust horizontal patterns versus height, and using SPCAM largely affects dust transport processes, which was seen in our simulations.

The zonal averaged DST04 versus height,

shown in Figure 4, reveals the DST04 pattern between SPCAM and CAM is different to a larger extent as compared to pattern from DST01 (Figure 2). Local maximum dust is still located in the lower layers around 10 °N - 40 °N, but DST04 in CAM reaches higher levels than SPCAM. There is a small plume of mixing ratio  $> 1e^{-8}$  kg/kg at 20 °N in the lowest layer shown in CAM but not seen in SPCAM. To understand the spatial dust distribution and the difference between SPCAM and CAM, the zonal mean mobilization and deposition flux at the surface are shown in Figure 5(a) and Figure 5(b), respectively. It is seen, overall, the mobilization flux between two simulations is very similar except at around 42 °N, the peak in SPCAM is higher than CAM about  $0.12 \mu \text{g m}^{-2} \text{s}^{-1}$ . However, the zonal averaged dry deposition flux from SPCAM is larger than CAM except from 0 to 10 °N where CAM predicts higher flux.

The vertical profile of the global mean dust mixing ratio is shown in Figure 6, where in the low troposphere near the surface, SPCAM predicts higher concentration of DST01, DST02, DST03. In the middle of the troposphere (950 mb - 700 mb), the averaged concentration is higher in CAM for all four dust bins. The higher mean dust values in CAM can reach to the 600 mb level for DST03, DST04. This implies using SPCAM to simulate dust evolution can modify the vertical distributions of dust, which can change the vertical profiles of solar and radiative energy. This would affect relevant cloud processes and cause modification of convection, cloud development, and interactions between clouds and the environment.

## 6. CONCLUSION

This study investigates the usage of superparameterization framework for dust transport processes. The sub-grid cloud and boundary layer processes are explicitly calculated by CRM in SPCAM and the distributions of dust are compared with distributions obtained from CAM, where the traditional parameterizations are used to represent sub-grid cloud systems. For one month of February, 2000 simulations, overall, the global patterns of DST01 are similar between CAM and SPCAM, but dust concentrations in SPCAM are slightly higher in areas near the source regions and the transported dust reaches to a longer distance than CAM. The zonal averaged DST01 profile shows the dust plume predicted by SPCAM

can reach high levels in the atmosphere but same plot for DST04 reveals the opposite that around local source areas from around 10 °N - 40 °N, DST04 in CAM is transported to higher altitudes than SPCAM. It is also seen SPCAM simulates a slightly higher mobilization flux for the 42 °N circle, and larger deposition fluxes for most of latitude circles excepts from 0 to 10 °N. The vertical profile of global mean dust concentration shows using SPCAM to simulate dust has the effect to redistribute vertical dust distributions and this can affect vertical profiles of solar and radiative energy. All of these processes would affect relevant cloud processes and may induces changes in small-scale, meso-scale and large-scale cloud systems and interactions between clouds and the environment.

## 7. ACKNOWLEDGEMENTS

This research was supported by the Center for Multiscale Modeling of Atmospheric Processes (CMMAP). We thank NCAR-CISL and TeraGrid-NICS for providing computer resources and Drs. Francis Vitt and Andrew Conley for their help in the CAM simulations.

## References

- [1] W. D. Collins, P. J. Rasch, B. A. Boville, J. J. Hack, J. R. McCaa, D. L. Williamson, B. P. Briegleb, C. M. Bitz, S.-J. Lin, and M. Zhang. The formulation and atmospheric simulation of the community atmosphere model version 3 (CAM 3). *J. Atmos. Sci.*, 19:2144–2161, 2006.
- [2] M. F. Khairoutdinov, C. DeMott, and D. A. Randall. Evaluation of the simulated interannual and subseasonal variability in an AMIP-style simulation using the CSU Multiscale Modeling Framework. *J. Climate*, 21:413–431, 2008.
- [3] M. F. Khairoutdinov and D. A. Randall. Cloud resolving modeling of the arm summer 1997 iop: Model formulation, results, uncertainties, and sensitivities. *J. Atmos. Sci.*, 60:607–625, 2003.
- [4] M. F. Khairoutdinov, D. A. Randall, and C. DeMott. Simulations of the atmospheric general circulation using a cloud-resolving model as a superparameterization of physical processes. *J. Atmos. Sci.*, 62:2136–2154, 2005.

- [5] David Randall, Marat Khairoutdinov, Akio Arakawa, and Wojciech Grabowski. Breaking the cloud parameterization deadlock. *Bull. Am. Met. Soc.*, 84:1547–1564, 2003.
- [6] Philip J. Rasch, Danielle B. Coleman, Natalie Mahowald, David L. Williamson, Shian-Jiann Lin, Byron A. Boville, and Peter Hess. Characteristics of atmospheric transport using three numerical formula-
- tions for atmospheric dynamics in a single GCM framework. *J. Climate*, 19:22432266, 2006.
- [7] Charles S. Zender, Huisheng Bian, and David Newman. Mineral Dust Entrainment and Deposition (DEAD) model: Description and 1990s dust climatology. *J. Geophys. Res.*, 108, D14:doi:10.1029/2002JD002775, 2003.

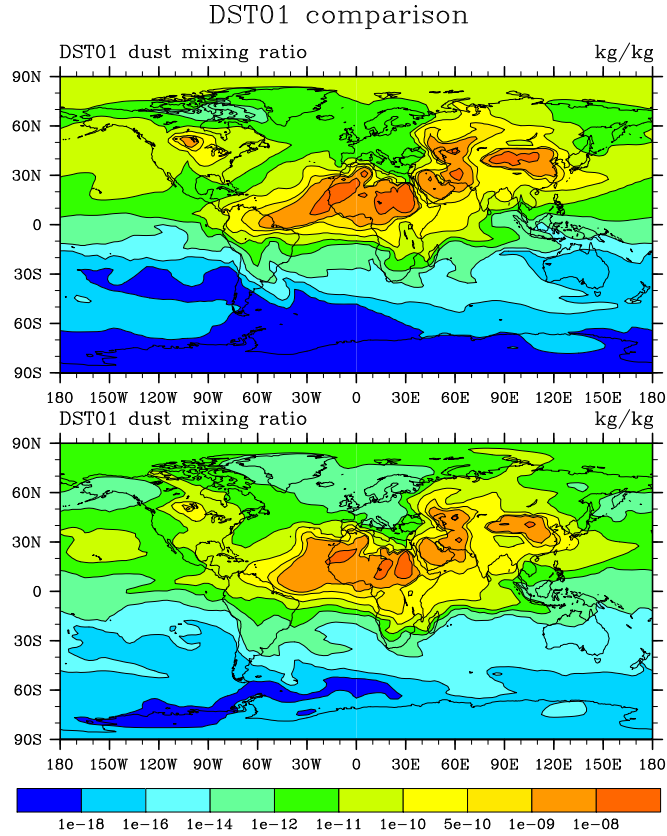


Figure 1: The global distribution of DST01 mixing ratio for the first model layer. Top is SPCAM, bottom is CAM. Unit is kg/kg.

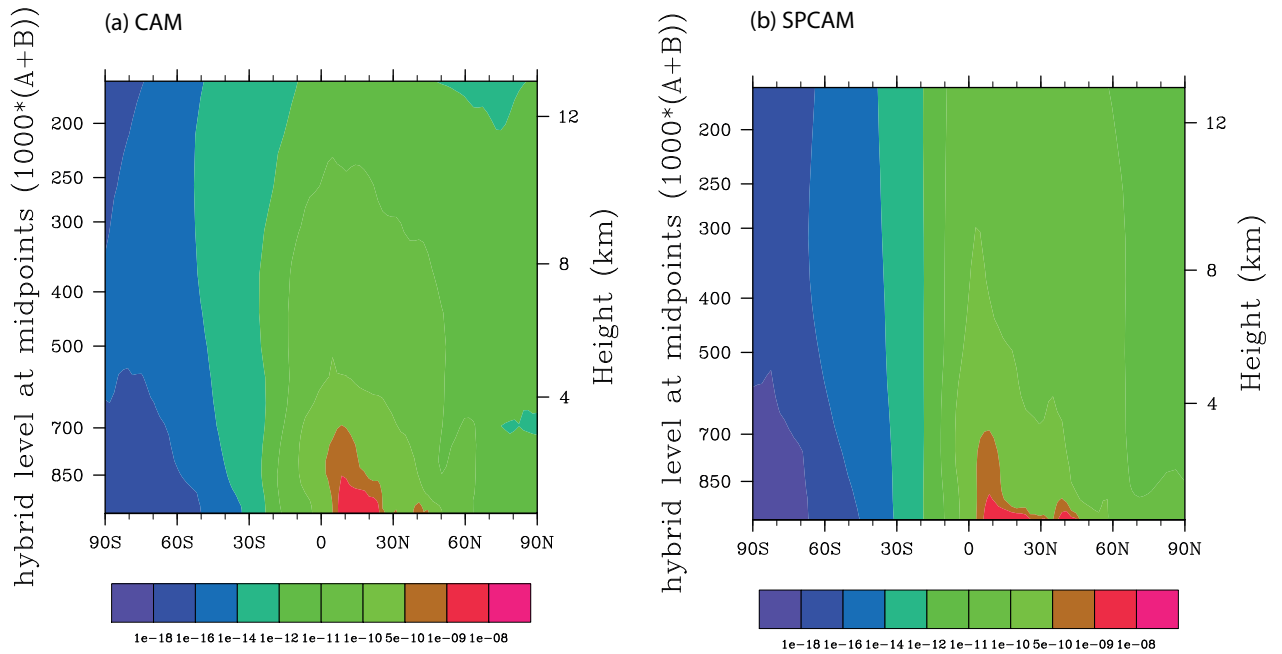


Figure 2: Zonal averaged DST01 versus height for (a) CAM and (b) SPCAM. Plots of DST01 are expressed in terms of mixing ratio, kg/kg.

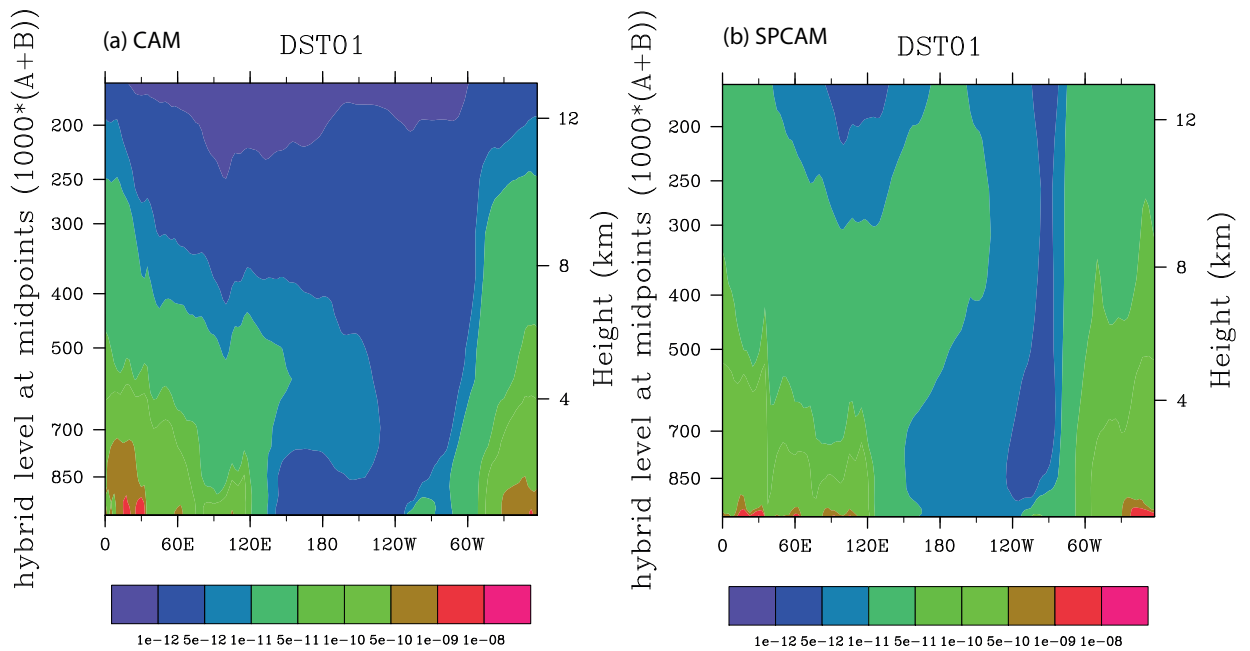


Figure 3: Meridional averaged DST01 versus height for (a) CAM and (b) SPCAM. Plots of DST01 are expressed in terms of mixing ratio, kg/kg.

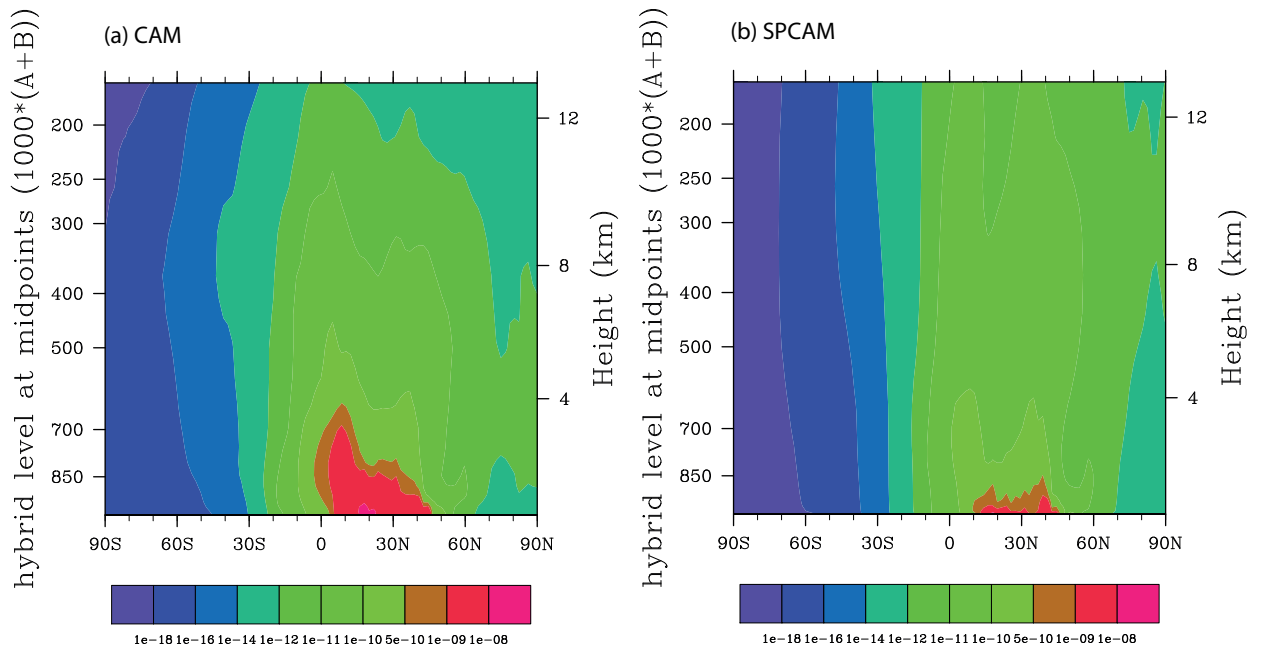


Figure 4: Zonal averaged DST04 versus height for (a) CAM and (b) SPCAM. Plots of DST04 are expressed in terms of mixing ratio, kg/kg.

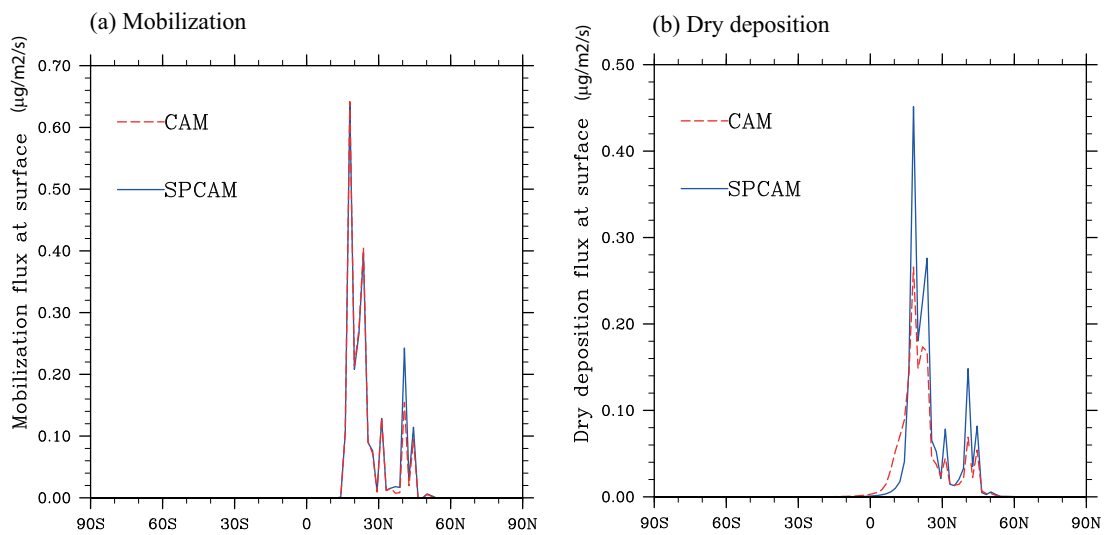


Figure 5: Zonal averaged dust profiles for CAM and SPCAM. (a) Mobilization surface flux and (b) Dry deposition surface flux. Unit of fluxes is  $\mu\text{g}/\text{m}^2/\text{s}$ .

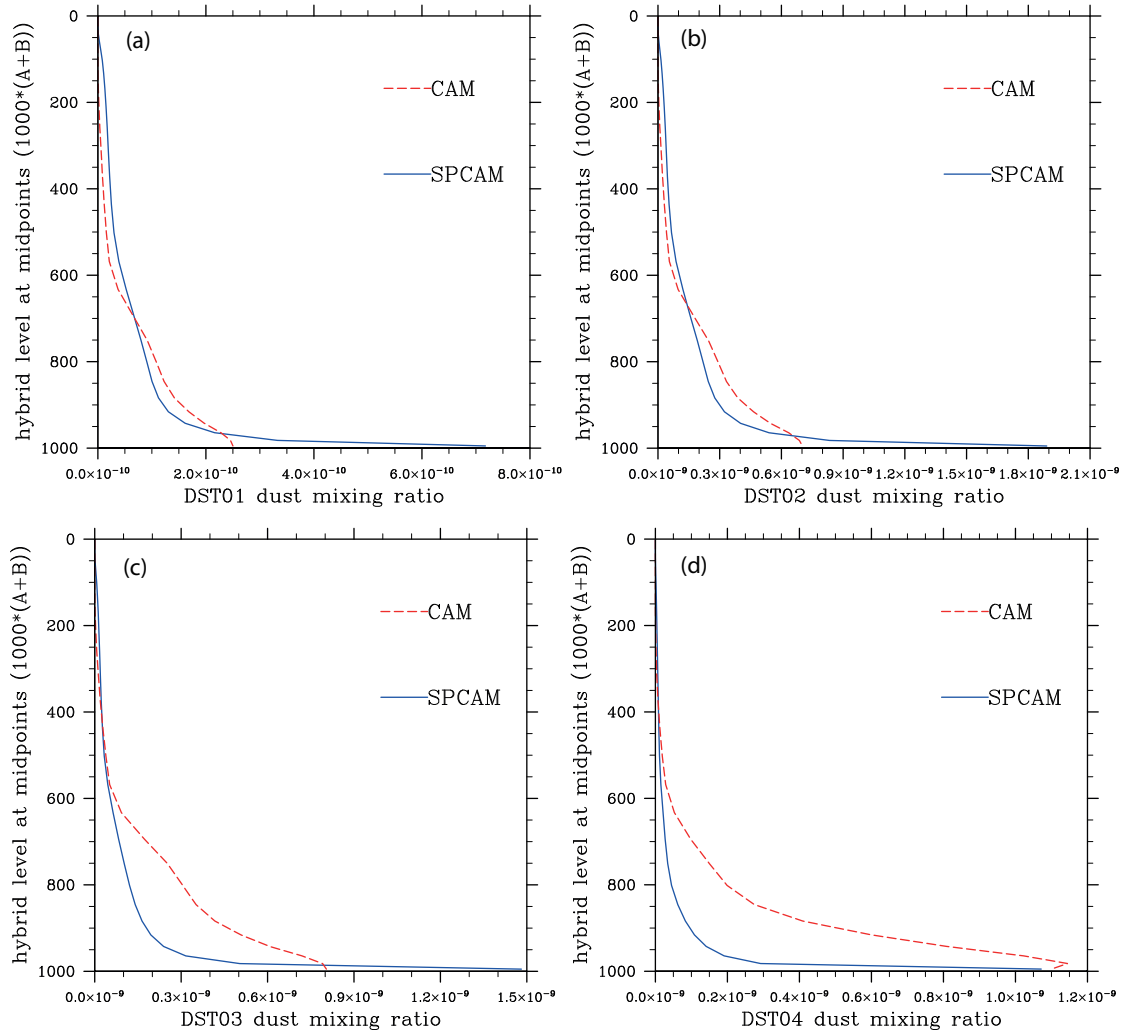


Figure 6: Global mean dust mixing ratio profiles for CAM and SPCAM. (a) DST01, (b) DST01, (c) DST03 and (d) DST04. Unit of mixing ratio is kg/kg.